OFFICE OF NAVAL RESEARCH

Contract N00014-91-J-1641

R&T Code 313W001

TECHNICAL REPORT NO. 71

Nickel Induced Defects and Their Role in Governing Chlorine Chemistry on the Si(100)

Surface

by

Z. Dohnálek, W. Yang, V.A. Ukraintsev, W.J. Choyke, and J.T. Yates, Jr.

Submitted To

Surface Science

19960701 007

Surface Science Center
Department of Chemistry
University of Pittsburgh
Pittsburgh, PA 15260

DTIC QUALITY INSPECTED 4

12 June 1996

REPORT DOCUMENTATION PAGE

Public reporting burden for this collection of information is estimated to average 1 hour per response, including the time for reviewing instructions, searching existing data sources, gathering and maintaining the data needed, and completing and reviewing the collection of information. Send comments regarding this burden estimate or any other aspect of this collection of information, including suggestions for reducing this burden, to Washington Headquarters Services, Directorate for Information Operations and Reports, 1215 Jefferson Davis Highway, Suite 1204, Arlington, VA 22202-4302, and to the Office of Management and Budget, Paperwork Reduction Project (0704-0188), Washington, DC 20503.

1. AGENCY USE ONLY (Leave blank)	2. REPORT DATE June 12, 1996	3. REPORT TYPE AND DATES COVERED Preprint

4. TITLE AND SUBTITLE

Nickel Induced Defects and Their Role in Governing Chlorine Chemistry on the Si(100) Surface

5. FUNDING NUMBERS

N00014-91-J-1641

6. AUTHOR(S)

Z. Dohnalek, W. Yang, V.A. Ukraintsev, W.J. Choyke and J.T. Yates, Jr.

7. PERFORMING ORGANIZATION NAME(S) AND ADDRESS(ES)

Surface Science Center
Department of Chemistry
University of Pittsburgh
Pittsburgh pA 15260

8. PERFORMING ORGANIZATION REPORT NUMBER

9. SPONSORING / MONITORING AGENCY NAME(S) AND ADDRESS(ES)

Office of Naval Research
Chemistry Division, Code 313
800 North Quincy Street
Arlington, Virginia 22217-5000

10. SPONSORING / MONITORING AGENCY REPORT NUMBER

11. SUPPLEMENTARY NOTES

12a. DISTRIBUTION / AVAILABILITY STATEMENT

12b. DISTRIBUTION CODE

13. ABSTRACT (Maximum 200 words)

The effect on chlorine surface chemistry of surface defects (split-off dimers) induced by controlled nickel contamination of Si(100) surfaces has been studied. It is shown that the mechanism of chlorine surface etching changes significantly with the presence of a small amount of split-off dimer defects (< 0.02 monolayer). A new defect-related low temperature $SiCl_2$ desorption channel is observed at ~ 550K, and the kinetics of the major $SiCl_2$ desorption channel at ~ 950K are changed. The presence of the low temperature $SiCl_2$ desorption is attributed to the existence of $SiCl_2$ surface species on the split-off dimer defects. The chlorine saturation coverage increases by up to ~ 10% in the studied range of defect densities. It is estimated that each split-off dimer defect contains 4.3 ± 0.6 extra chlorine atoms compared to the ideal chlorine-saturated Si(100) surface. On non-defective Cl-dosed Si(100) surfaces, the electron stimulated desorption ion angular distribution (ESDIAD) images show only four off-normal Cl^+ beams. With increasing defect density a new Cl^+ beam develops in the normal <100> direction. This feature is associated with the Cl bonding on the split-off dimer defects, and is similar to that produced on Si(100) surface containing point defects created in other ways.

14. SUBJECT TERMS

Silicon (100)	Nickel	Electron Stimulated
Surface defects	Chemisorption	Desorption Ion Angular
Chlorine	Etching	Distribution

15. NUMBER OF PAGES

16. PRICE CODE

17. SECURITY CLASSIFICATION OF REPORT	18. SECURITY CLASSIFICATION OF THIS PAGE	19. SECURITY CLASSIFICATION OF ABSTRACT	20. LIMITATION OF ABSTRACT

Nickel Induced Defects and Their Role in Governing

Chlorine Chemistry on the Si(100) Surface

Z. Dohnálek, W. Yang[†], V. A. Ukraintsev, W. J. Choyke[†], and J. T. Yates, Jr.

University of Pittsburgh
Department of Chemistry
Surface Science Center
Pittsburgh, PA 15260

† University of Pittsburgh
Department of Physics
Pittsburgh, PA 15260

1

Nickel Induced Defects and Their Role in Governing

Chlorine Chemistry on the Si(100) Surface

Z. Dohnálek, W. Yang[†], V. A. Ukraintsev, W. J. Choyke[†], and J. T. Yates, Jr.

University of Pittsburgh
Department of Chemistry
Surface Science Center
Pittsburgh, PA 15260

† University of Pittsburgh
Department of Physics
Pittsburgh, PA 15260

Abstract

The effect on chlorine surface chemistry of surface defects (split-off dimers) induced by controlled nickel contamination of Si(100) surfaces has been studied. It is shown that the mechanism of chlorine surface etching changes significantly with the presence of a small amount of split-off dimer defects (< 0.02 monolayer). A new defect-related low temperature $SiCl_2$ desorption channel is observed at ~ 550K, and the kinetics of the major $SiCl_2$ desorption channel at ~ 950K are changed. The presence of the low temperature $SiCl_2$ desorption is attributed to the existence of $SiCl_2$ surface species on the split-off dimer defects. The chlorine saturation coverage increases by up to ~ 10% in the studied range of defect densities. It is estimated that each split-off dimer defect contains 4.3 ± 0.6 extra chlorine atoms compared to the ideal chlorine-saturated Si(100) surface. On non-defective Cl-dosed Si(100) surfaces, the electron stimulated desorption ion angular distribution (ESDIAD) images show only four off-normal Cl^+ beams. With increasing defect density a new Cl^+ beam develops in the normal <100> direction. This feature is associated with the Cl bonding on the split-off dimer defects, and is similar to that produced on Si(100) surface containing point defects created in other ways.

I. Introduction

It is well known that the preparation of the Si(100)-(2×1) surface with a low defect density is a process which is very difficult to control [1]. It was shown by scanning tunneling microscopy (STM) that great care has to be taken to avoid any possible sources of contamination leading to defect production. High surface concentrations of carbon, the use of sputtering for surface cleaning [2-4], the application of nickel-containing thermocouples for temperature measurement [4], and the use of stainless steel parts on a crystal mount [5] are examples which ultimately lead to high surface defect densities and finally to surface roughening. The most critical problem is nickel contamination [4-8]. Even very low levels of nickel contamination which are barely detectable by Auger electron spectroscopy (AES) are sufficient to produce high defect densities and finally to roughen the Si(100) surface. This leads to asking of an important question, addressed in this paper. How does one check the surface quality of Si(100)-(2×1) in experimental systems lacking atomically resolved (STM) monitoring of the surface conditions?

In this paper we show an example of Si(100) surface chemistry which is extremely sensitive to the defects intentionally prepared on the Si(100) surface. This specific chemistry can be used as an indicator of the presence of Si(100) surface defects.

It was first shown by low energy electron diffraction (LEED) studies of the Si(100)-(2×1) surface that a small amount of nickel impurity (AES peak ratio $Ni_{(LMM)}/Si_{(LVV)} \approx 0.004 - 0.010$ corresponding to $\theta_{Ni} \approx 0.06 - 0.15$ monolayer (ML) in the depth of Auger sampling [4]) leads to the formation of (2×n) superstructures [6, 7]. With the invention of the STM these superstructures were observed directly in real space and were found to be due to channels of the Si-Si dimer vacancies running perpendicular to the direction of the dimer rows [4, 5, 8]. The exact location of nickel atoms is still uncertain but it is believed that they are present in the sub-surface region rather than on the surface [4, 8]. For lower concentrations of nickel impurities ($Ni_{(LMM)}/Si_{(LVV)} < 0.002$) the defects are isolated with each defect affecting an area composed of six surface dimers (Figs. 1b and 1c) on an ideal dimer row (Fig. 1a). As a result of its characteristic sequence - a dimer vacancy - a dimer - a double dimer vacancy - it was named the split-off dimer defect. The structure of the split-off dimer defect was first proposed by Niehus et al. [8] based on their STM results (Fig. 1b). Subsequent theoretical calculations and STM studies proposed the reconstruction of the silicon atoms inside of the dimer vacancy and the double dimer vacancy producing the structure as suggested by Wang et al. [9] and others [10, 11] (Fig. 1c).

A quantitative linear relationship between the surface concentration of the split-off dimer defects and the $Ni_{(LMM)}/Si_{(LVV)}$ AES peak ratio was determined in a STM study by Ukraintsev and Yates [4]. Their data are in agreement with the

4

dependence between the spacing of vacancy channels (n) in a (2×n) reconstruction observed by LEED and correlated with the $Ni_{(LMM)}/Si_{(LVV)}$ AES peak ratio [6]

The reaction of chlorine on the Si(100)-(2×1) surface is one of the most intensively studied reactions on this surface [12-27]. The reason for this interest has to do with the industrial importance of this system, since chlorine-based etching is widely employed. Many studies of the Cl/Si(100) system reveal discrepancies which are unexplained at present and are likely to be due to lack of control of defect density. Two examples of different experimental results or different interpretations of the results are outlined below.

The first example of variable results involves the desorption of reaction products upon heating a chlorine-saturated Si(100) surface. A general conclusion from all the studies is that $SiCl_x$ species (x = 1-4) are the reaction products, causing etching [14, 17-21, 28]. Two desorption processes are observed upon heating of the chlorine-saturated Si(100) surface, a low temperature one at ~ 500K and a high temperature one at ~ 900K. The relative contribution of these processes varies significantly from study to study. In some studies the peak area of the low temperature desorption process is comparable to the peak area of the high temperature desorption process [17, 19]; in other studies the low temperature desorption process is only ~ 10% of the total desorption peak area [14, 20]. Thus the relative yield of the two thermal etching processes varies widely from study to

study. We believe this is due to the variation of surface defect levels in the various experiments.

The second example where different interpretations have been advanced has to do with the silicon - chlorine bonding configuration proposed, based on measurements made by the electron stimulated desorption ion angular distribution (ESDIAD) technique. The Cl^+ ESDIAD images show two types of features depending on the annealing temperature: a Cl^+ beam in the normal <100> direction and four Cl^+ beams in the off normal directions [14, 23, 29, 30]. The temperature range of existence of the normal Cl^+ beam varies in different studies. Two interpretations of the normal Cl^+ beam exist. In the first interpretation, a symmetrical bridge-bonded Cl atom bonded to two Si atoms is proposed to yield a normal Cl^+ ESDIAD beam as two equivalent Si-Cl bonds are ruptured in ESD giving a normal ejection force on the Cl^+ species [14, 29]. In the second interpretation, a normally-oriented Si-Cl single bond is proposed to be present at a buckled Si-Si dimer site and to yield a normal Cl^+ beam [23, 30]. The off normal beams are universally interpreted as the Cl^+ desorption from chlorine atoms terminally bonded to the dangling bonds of Si-Si dimers [14, 23, 29, 30].

In this work we study the effect of controlled low level nickel contamination on the chlorine-derived chemistry observed on the Si(100)-(2×1) surface. Defects are induced by Ni on the surface. Temperature programmed desorption (TPD) results show that the intensity of the low-temperature $SiCl_2$

desorption process is correlated with the defect concentration and that the desorption kinetics of the high temperature $SiCl_2$ desorption process are changed as a result of Ni-induced defects. We conclude that the chlorine saturation coverage significantly increases with increasing defect density, and that each split-off dimer defect ensemble adsorbs approximately four additional chlorine atoms relative to the ideal surface. The normal Cl^+ beam in ESDIAD is not seen at any chlorine coverage on the non-defective Si(100) surface. On the defective Si(100) surface the normal beam intensity is proportional to the nickel surface concentration.

II. Experimental

The experiments were conducted in an ultra-high vacuum (UHV) chamber with a base pressure of $\sim 3 \times 10^{-11}$ Torr. This UHV chamber was equipped with a cylindrical mirror analyzer (CMA) Auger electron spectrometer (AES), an argon-ion sputtering gun, a digital LEED/ESDIAD apparatus, a shielded quadrupole mass spectrometer (QMS) for line-of-sight temperature programmed desorption (TPD) experiments, and an additional QMS coupled with an electron gun for ion mass analysis during electron stimulated desorption (ESD) processes. In addition a Ni evaporation source was present.

In all experiments, Si(100) wafers purchased from Virginia Semiconductors, Inc. were used (floating zone grown, p-type, boron doped,

5 - 20 Ωcm, 0.4mm thick, miscut angle < 0.5°, one side polished). Crystals of desired size (23×12 mm^2) were cut using a diamond cutter, sonicated in methyl alcohol (spectrophotometric grade), rinsed for several minutes in deionized water ($\sim 10^{18}$ Ωcm), and mounted on the manipulator. A special crystal mounting structure was used in which Si wafer contacts under compression were used to clamp each end of the crystal, leading to high homogeneity of temperature across the crystal. A more detailed description of this mounting will be published elsewhere [31].

Crystal temperature measurements were performed using a W26%Re/W5%Re thermocouple. The thermocouple was inserted into a thin Ta tube (Goodfellow Cambridge Limited, OD = 0.31mm) to prevent direct contact with the crystal. The tube was flattened, bent into a U shape, and clipped on the edge of the crystal [31]. The temperature reading was checked using an optical pyrometer at a wavelength of 0.65μm. At $\sim$ 1400K the pyrometer reading (corrected for Si emissivity and transmission through the window) was 100K higher than the thermocouple reading.

The Si(100) surface was initially cleaned by high temperature annealing ($\sim$ 1410K, 60s) followed by fast cooling ($\sim$ 20K/s) to 973K and slow subsequent cooling ($\sim$ 2K/s) to $\sim$ 120K. This procedure was used for the surface preparation before every experiment. The surface cleanliness was checked using AES spectroscopy with a detection limit (noise/Si$_{(LVV)}$) better than 0.001. Except for the

8

silicon features, only a small carbon (KLL) peak at 272eV was detected with an intensity of ~ 0.001 relative to the intensity of the silicon (LVV) peak. The presence of the (2×1) reconstruction was confirmed using LEED.

The nickel atoms were evaporated onto the crystal from a resistively heated high purity nickel wire (Johnson Matthey, 99.9945%). The wire was folded into a large area coil $(10 \times 10 \text{ mm}^2)$ to ensure homogeneous nickel coverage on the Si(100) surface. The coil was thoroughly shielded by a tantalum shield to prevent undesired nickel deposition. Each evaporation cycle was followed by crystal annealing to 1410K for 60s.

Chlorine gas (Matheson, 99.999%) was further purified by several freeze - pump - thaw cycles and introduced through passivated stainless steel tubing and valves to the chamber through a multicapillary array doser delivering a known Cl_2 flux to the crystal [32, 33].

All Cl^+ ESDIAD images were obtained at a crystal temperature $\sim 120K$ using +15V bias voltage on the crystal and an incident electron energy of 120eV. The effect of the structureless background (due to soft X-rays) was minimized by subtraction of the pattern obtained in the configuration where all positive ions are retarded in the ESDIAD analyzer. Final ESDIAD images were smoothed for presentation purposes using 5-point polynomial smoothing function [34].

III. Results

A. SiCl$_2$ Desorption from Defective Si(100)

The SiCl$^+$ (m/e$^-$ = 63$^+$) TPD spectra from chlorine-saturated Si(100)-(2×1) surfaces are presented in Figure 2. The full range of SiCl$_X$(g) species (x = 1 - 4) desorbing from chlorine-saturated Si(100) surface has been observed previously with SiCl$_2$ as the dominant desorption product [14, 17-21, 28]. In our experiments SiCl$^+$ and SiCl$_2^+$, and SiCl$_3^+$ ions were monitored but only SiCl$^+$ and SiCl$_2^+$ were observed. Both ions show the same temperature dependence and most probably come from the ionization of the parent SiCl$_2$(g) molecule.

The TPD spectrum from the non-defective Si(100) surface (Fig. 2a) reveals two SiCl$_2$ desorption features. The first feature occurs at ~ 550K (2% of total desorption area), and the second occurs at ~ 930K (98% of total desorption area). Upon adding Ni and annealing to produce surface defects (Fig. 2b-e), the following changes in the TPD spectra were seen:

(a) The area of low temperature SiCl$_2$ desorption peak increases. Comparing Figs. 2a and 2e the area increases from 2% to 10% of the total desorption yield.

(b) The high temperature SiCl$_2$ desorption peak significantly broadens and its peak maximum shifts to lower temperature. Comparing Figs. 2a and 2e the FWHM increases from 26K to 56K and the maximum shifts from 929K to 898K.

10

The SiCl$^+$ desorption areas observed in TPD as a function of nickel exposure are shown in Figure 3a. The areas are reported relative to the total SiCl$^+$ desorption area from the non-defective Si(100) surface (1.00 ± 0.02). The total area of SiCl$^+$ desorption increases by ~ 10% (open circles) at the highest nickel concentration where the Ni$_{(LMM)}$/Si$_{(LVV)}$ ratio was still less than 0.002, corresponding to about 3.0% of a monolayer of Ni [4]. The filled circles represent the SiCl$^+$ TPD area above 750K which measures only the area of the high temperature desorption peak (see Figure 2). It can be seen that the SiCl$_2$ yield in the high temperature process is virtually constant within the error of our experiment for the whole range of nickel concentrations studied.

To confirm the increase of the chlorine saturation coverage by another analytical technique we also show in Fig. 3a the data (two points) obtained by AES studies of the saturated Cl coverage (empty squares). It can be seen that the Cl coverage increase due to Ni induced defects closely follows the fractional increase obtained from the SiCl$^+$ TPD areas. The normalized Cl$_{(LMM)}$/Si$_{(LVV)}$ AES peak ratios in the two experiments corresponding to non-defective Si(100) (Figure 2a) and highly defective Si(100) (Figure 2e) are 1.00 ± 0.02 and 1.10 ± 0.01, respectively. The standard deviations are calculated by averaging results from three independent measurements. Thus both TPD studies of SiCl$_2$ desorption and AES studies of the saturated layer indicate that the range of defect

densities studied in this paper cause a ~ 10% increase in the Cl saturation coverage.

The dependence between the relative $SiCl^+$ desorption area of the low temperature $SiCl_2$ peak and the nickel concentration (from the $Ni_{(LMM)}/Si_{(LVV)}$ AES peak ratio) is shown in Figure 3b (triangles). The horizontal error bars are estimated from the ratio of noise to the intensity of the $Si_{(LVV)}$ AES peak. The solid line represents a linear regression through the data. A data point shown as a gray triangle is not considered for the regression since the $Ni_{(LMM)}/Si_{(LVV)}$ AES peak ratio is below the detection limit of our instrument and could not be measured directly. Its abscissa was determined using the fit of the $Ni_{(LMM)}/Si_{(LVV)}$ AES ratio dependence on the nickel evaporation time. These data suggest that the excess Cl coverage due to defects is linearly related to the impurity Ni coverage producing these defects.

B.   ESDIAD Results

The three-dimensional Cl^+ ESDIAD images for different chlorine coverages on a non-defective Si(100)-(2×1) surface (no Ni deposit) are shown in Figure 4. The images are taken immediately after chlorine adsorption at ~ 120K. The plots are shown with equidistantly spaced Z contours and a gray scale. The Z scale, contour spacing, and gray scale are the same for all images. The chlorine coverage

is measured as the $Cl_{(LMM)}/Si_{(LVV)}$ Auger peak ratio and normalized to the saturation coverage.

Figure 4 shows that four off-normal Cl^+ beams are observed for the entire range of chlorine coverages. The Cl^+ yield reaches a maximum for a relative chlorine coverage ~ 0.3ML, and for higher coverages the Cl^+ yield monotonically decreases to almost zero for saturation coverage. This effect is due to self-quenching between neighbor Cl atoms causing the ion yield to maximize at intermediate coverages [14].

The effect of nickel contamination and subsequent defect production on the Cl^+ yield and the angular distribution of Cl^+ ion emission from Si(100) surfaces for two different chlorine coverages is shown in Fig. 5A (Cl saturation coverage, here defined as 1ML) and Fig. 5B (~ 0.25 ML of Cl/Si(100)). The example of a Cl^+ ESDIAD pattern for the most defective surface is presented as an inset in Figure 5A. The pattern is shown as a gray scale image with white and black regions corresponding to zero and to maximum Cl^+ ion counts, respectively. The solid lines in Figures 5A and 5B are vertical sections taken from the Cl^+ ESDIAD images along the <011> direction. They show a development of the normal Cl^+ beam with increasing defect density after the chlorine adsorption at ~ 120K. A Cl-saturated non-defective surface (Fig. 5A, line a) yields a very weak Cl^+ signal. As the amount of nickel increases (Fig. 5A, lines b - d) the maximum in the normal direction becomes apparent and the Cl^+ yield increases significantly. The same

13

trend can be seen in Figure 5B for a low Cl coverage (0.25ML) where diminished

Cl···Cl neighbor quenching occurs [14].

IV. Discussion

A. Saturation Chlorine Coverage and Defect Density

As shown in Figure 2, the $SiCl_2$ desorption spectra from Si(100) surfaces

containing full coverages of Cl change significantly with increasing nickel

contamination followed by annealing to induce defect formation: 1) the low

temperature desorption peak develops; 2) the high temperature desorption peak

broadens and its maximum shifts to the lower temperatures. All of these changes

are directly related to the presence of the nickel-induced defects which yield

split-off dimer STM patterns [4, 5, 8]. The extremely narrow high temperature

$SiCl_2$ desorption peak from the non-defective Si(100) surface (spectrum a,

FWHM = 26K) is unusual for such a high temperature and represents an example

of "explosive" desorption kinetics. More detailed analysis of the desorption

kinetics for this process on the non-defective Si(100) surface is the subject of

another paper [35]. Desorption spectra similar to spectrum d) and e) are obtained

not only on Si(100) with nickel induced defects, but also on Si(100) with defects

created by gentle low energy Ar^+ sputtering [36], or even on Si(100) surfaces with

higher levels of carbon contamination ($C_{(KLL)}/Si_{(LVV)} > \sim 0.003$). These desorption

spectra closely resemble the spectra presented in the previous studies [14, 20], and are undoubtedly due to uncontrolled defects present on these surfaces.

If we analyze the total normalized $SiCl^+$ thermal desorption area from Figure 2 we see a significant increase of the total $SiCl^+$ yield and hence the total chlorine coverage as a function of increasing nickel-induced defect density (open circles in Figure 3a). To confirm the increase of the saturation chlorine coverage by another measurement technique we also measured the $Cl_{(LMM)}/Si_{(LVV)}$ AES peak ratio for the non-defective and the most defective surfaces (empty squares in Fig. 3a). The same fractional increase of saturation chlorine coverage (approx. 10%) is observed, confirming our coverage studies using TPD. It is interesting to notice that the area of the high temperature $SiCl^+$ desorption peak remains constant $(1.00 \pm 0.02$ ML) over the whole range of defect densities.

Using the relative area of low temperature $SiCl^+$ desorption peak as a measure of the amount of excess chlorine and the assumption that the chlorine saturation coverage on the ideal Si(100)-(2×1) surface is one chlorine per surface silicon atom $(6.78 \times 10^{14}$ cm$^{-2})$ we are able to estimate the number of extra chlorine atoms for each split-off dimer. The dependence of the amount of excess chlorine on the $Ni_{(LMM)}/Si_{(LVV)}$ AES peak ratio and estimated atomic fraction of the nickel is shown in Fig. 3b. Using the linear regression (solid line) and a previously published correlation between the density of split-off dimers and the $Ni_{(LMM)}/Si_{(LVV)}$ AES peak ratio [4], we estimate that there are 4.3 ± 0.6 extra

15

chlorine atoms per every split-off dimer defect site originally composed of 4 normal silicon dimers. The standard deviation includes the error of the linear regression from Figure 3b, the error of the normalization of the $SiCl^+$ desorption area, and the error of the dependence of the split-off dimer density on the $Ni_{(LMM)}/Si_{(LVV)}$ AES peak ratio.

By counting the number of dangling bonds on the models presented in Figs. 1a - 1c we can see that by saturation of these dangling bonds one gets 8 chlorine atoms for four dimer sites on the ideal surface (Fig. 1a), 14 chlorine atoms (6 extra) on Niehus's split-off dimer defect site (Fig. 1b), and 6 chlorine atoms (2 less) on Wang's split-off dimer defect site (Fig. 1c). These two models can be considered as an upper (Niehus) and lower limit (Wang) for the change of chlorine saturation coverage with respect to the saturation coverage of the ideal surface. Since our data show the increase of the chlorine coverage on the defective surfaces (4.3 ± 0.6 extra Cl per split-off dimer defect) we conclude that the chlorine saturated structure of the split-off dimer defect corresponds to the structure with the internal Si-Si rebonding broken. Since Si-Si rebonding occurs in Wang's model, the measurement of excess Cl on the defective surface favors Niehus' model for the split-off dimer defect, or suggests that the rebonding in the Wang's model is broken upon Cl_2 adsorption.

As a possible reason for the development of low temperature $SiCl_2$ desorption feature on the defective surface, we postulate the existence of the

surface dichloride species on the defects. This can occur by direct chlorine adsorption on the double dimer vacancy of Niehus's split-off dimer defect (formation of one dichloride species in Figure 1b), or by breaking of the reconstruction of the double dimer vacancy in Wang's split-off dimer defect (formation of two dichloride species in Figure 1c) upon chlorine adsorption. The activation barrier for the desorption of the $SiCl_2$ from surface dichloride species is probably lower than the activation barrier for desorption of $SiCl_2$ from surface monochloride species [37-39]. There is also supporting evidence for the presence of a minority of dichloride species on the Si(100) surface from the XPS study by Durbin et al. [24].

B.   Origin of Cl^+ Emission in <100> Normal Direction

In this section we discuss the origin of the Cl^+ beam emitted in the normal <100> direction as observed in Cl^+ ESDIAD images. As already mentioned this prominent normal beam was observed previously in many Cl^+ ESDIAD studies including ours [14, 23, 27, 29, 30]. With significant improvement of the silicon surface preparation technique [31], initiated as a result of our STM studies [4], we do not observe normal Cl^+ emission from the non-defective Si(100) surface. This is illustrated in Figure 4 in the Cl^+ ESDIAD images over the whole range of chlorine coverage obtained after the dosing the non-defective Si(100) surface at ~ 120K.

The Cl$^+$ ESDIAD images after chlorine saturation at ~ 120K for different levels of nickel concentration are shown in Figures 5A and 5B. For easier comparison the data are presented as cuts along the <011> direction rather than complete two dimensional images. An example of a full image for the highest level of defect density studied (Ni(LMM/Si$_{(LVV)}$)= 0.0060) is shown as an inset. The development of the normal Cl$^+$ beam with the increasing defect density is apparent. The total Cl$^+$ yield increases by a factor of 5, going from the non-defective surface (line a) to the most defective surface (line d) in Figure 5a. This demonstrates a direct relationship between the concentration of the defects and the intensity of the normal Cl$^+$ beam.

Based on the direct evidence presented in Figures 5A and 5B, we conclude that the normal Cl$^+$ emission comes from chemisorbed Cl associated with the defect sites. It should be mentioned that the existence of this normal Cl$^+$ beam is not specifically related only to the defects induced by the nickel contamination. We have observed the same type of normal Cl$^+$ emission on the Si(100) surfaces with the defects introduced by gentle sputtering [36] or by chlorine etching [14, 27]. The puzzling question is what type of the local chlorine bonding will produce the Cl$^+$ emission in the normal direction. Two explanations are possible, and our current experimental data are not capable of resolving this question. In the next part of the discussion we present two possible models for the origin of a normal Cl$^+$ ESDIAD beam from Cl adsorbed on Si dimer vacancy defect sites.

The common point for all types of defective surfaces mentioned above is the formation of dimer vacancies and their further growth into the dimer vacancy channels and islands as observed by many STM studies [4, 5, 8, 22, 40-42]. We conclude that these dimer vacancies play an important role in the formation of the surface species yielding the normal Cl^+ beam in ESDIAD.

We start with the discussion of the basic building block of all larger dimer vacancy clusters - a single dimer vacancy. There are two possible ways to saturate the single dimer vacancy with chlorine. Both configurations can be a possible source of the normal Cl^+ emission.

1.   Model A - Bridged Cl on Si Dimer Vacancy Site

The first model for a surface structure providing a normal Cl^+ beam involves saturating the dimer vacancy with two chlorine atoms in the bridging positions producing symmetrically bonded Cl atoms (Figure 6a). There are theoretical studies showing a local energetic minimum for the Si(100) surface saturated with the bridge bonded chlorine atoms (dimerization is broken in this case). It was calculated that this metastable structure is significantly less favorable (by 0.96 eV) than the silicon dimer reconstruction saturated with terminally bonded chlorine [25]. The question of how the energetics of these two possible configurations (terminally and bridge bonded chlorine) compare inside of the dimer vacancy remains to be calculated since the chlorine bridge bonding inside of

the dimer vacancy is not at all energetically equivalent to the bridge bonding situation on the non-defective Si(100)-(2×1) surface.

2. Model B - Terminal Si-Cl bonds undergoing repulsion

The second model for Cl adsorption on a defect site yielding a normal Cl^+ beam in ESDIAD involves the adsorption of four terminally bonded chlorine atoms on the four Si dangling bonds at a dimer vacancy defect site (Figure 6b). In the simple geometric picture this will bring the chlorine atoms on the opposite sides of the dimer vacancy into very close proximity at a distance of ~2.5Å. (estimate based on the silicon - silicon distance in the dimer vacancy 3.84Å, length of the Si-Cl bond 2.05Å [25], and its 19.5° tetrahedral inclination from the normal). Since the length of the Cl-Cl bond in the molecule is 1.99Å we expect that there will be a repulsion between the non-bonded chlorine atoms at such a close distance as ~2.5Å. This would lead to the significant decrease of the ideal tetrahedral angle (19.5°), and possibly to Cl^+ emission directions close to the normal direction. A sum of four emission directions from two orthogonal domains of Si-Si dimer terraces present on all Si(100) crystals, may give a composite Cl^+ ESDIAD pattern with the maximum in the normal direction.

3. SiCl₂ Surface Species

We now consider the smallest dimer vacancy cluster - a double dimer vacancy. As already mentioned there is a possibility of formation of dichloride

surface species as may be seen in Figure 1b. This suggests the possibility of Cl^+ ion desorption from these $SiCl_2$ species. Based on the ideal tetrahedral structure the inclination angle from the surface normal for Si-Cl bonds of $SiCl_2$ species would be 55°. This is much higher than the critical escape angle for Cl^+ ions [14] and we therefore do not expect to see them by ESDIAD. The experimental evidence for absolute quenching of Cl^+ from higher chlorides is presented elsewhere for the chlorine-saturated Si(111)-(7×7) surface [43].

V.   Conclusions

In this study, we have shown the effect of low concentration of the nickel-induced defects (split-off dimers) on the chlorine chemistry of the Si(100)-(2×1) surface as observed by TPD, AES, and ESDIAD techniques.

The TPD experiments show significant changes in the mechanism of the chlorine etching on the defective Si(100) surfaces as compared to the non-defective Si(100) surface. A new low temperature $SiCl_2$ desorption feature develops at ~ 550K, and the amount of $SiCl_2$ species desorbing via this low energy process is directly proportional to the density of Ni-induced split-off dimer defects. We postulate that this desorption process is associated with the presence of $SiCl_2$ surface species on these defects. In addition, changes in the kinetics of the evolution in the main $SiCl_2$ desorption process (at ~ 950K) are observed.

We observe an increase of total Cl saturation coverage on defective Si(100) surfaces (~ 10% increase for ~ 0.017ML of split-off dimer defects). Based on the correlation among the density of split-off dimer defects, the $Ni_{(LMM)}/Si_{(LVV)}$ Auger peak ratio, and the Cl excess coverage, we estimate that there are 4.3 ± 0.6 extra chlorine atoms on every split-off dimer defect compared to the same area of the ideal Cl-saturated Si(100) surface.

In our ESDIAD experiments only four off normal Cl^+ beams are observed on non-defective Si(100) after Cl adsorption at ~ 120K. The directions of the Cl^+ beams correspond to the terminal bonding of Cl atoms on the dangling bonds of Si-Si dimers. In contrast, on defective Si(100) surfaces, a normal beam of Cl^+ emission develops as the split-off dimer defect density increases. This Cl^+ ESDIAD feature is associated with Cl bonding on the split-off dimer defect sites. The appearance of the normal Cl^+ ESDIAD beam and the low temperature $SiCl_2$ desorption process serve as a method for the evaluation of the Ni induced defect distribution on Si(100) surfaces.

Acknowledgment

Fellowship. Another acknowledges the International Union of Vacuum Science and Technology for the Award of a Welch Scholarship.

Figure Captions

Figure 1. A schematic top view of a Si-Si dimer row showing: (a) an ideal surface; (b) a split-off dimer defect proposed by Niehus et al. [8]; (c) a split-off dimer defect by Wang et al. [9]. The height of the atoms is shown by gray scale filling of the circles where black represents the top layer and white the bottom layer. The surface dangling bonds are shown as ovals with black dots, representing a single electron.

Figure 2. The SiCl$^+$ TPD spectra from chlorine-saturated Si(100) surfaces for: (a) non-defective surface; (b) - (e) defective surfaces with the exposure to the nickel evaporation source being 2min, 10min, 30min, and 120min, respectively. All spectra were acquired with a temperature ramp of 2K/s.

Figure 3. (a) The dependencies of relative amount of surface chlorine as a function of nickel exposure time measured by SiCl$_2$ TPD; empty circles: total SiCl$^+$ area; black circles: SiCl$^+$ area above 750K, empty squares: normalized Cl$_{(LMM)}$/Si$_{(LVV)}$ AES peak ratios. The dependencies are normalized with respect to the data obtained from a non-defective surface.

(b) The amount of excess chlorine on the saturated Si(100) surface as a function of Ni$_{(LMM)}$/Si$_{(LVV)}$ AES peak ratio. The data are obtained from the SiCl$^+$ desorption areas below 750K, ratioed to the total SiCl$^+$ desorption area from the non-defective surface.

Figure 4. Three-dimensional Cl⁺ ESDIAD images from a chlorine-dosed non-defective Si(100-(2×1) surface. The images correspond to different chlorine coverages as measured by $Cl_{(LMM)}/Si_{(LVV)}$ AES peak ratios. The coverages are normalized with respect to the saturation coverage: (a) 0.07ML; (b) 0.29ML; (c) 0.71ML; (d) 1.00ML. Z scale, contour spacing, and gray scale are the same for all images.

Figure 5. The cuts through Cl⁺ ESDIAD images in the <011> direction after the chlorine adsorption at 120K to saturation coverage = 1.00ML (Figure 5A) and 0.25ML (Figure 5B). Line a: non-defective surface; lines b - d: defective surfaces with nickel concentration measured as $Ni_{(LMM)}/Si_{(LVV)}$ AES peak ratios equal to 0.0011, 0.0020, and 0.0060, respectively. The corresponding calculated Ni coverages are 0.02, 0.03, and 0.09 ML in the depth of Auger sampling. A contour representation of the entire Cl⁺ ESDIAD image is shown as an inset in Figure 5A.

Figure 6. A schematic top view of a single dimer vacancy defect showing a model of: (a) Cl bridge-bonding; and (b) Cl terminal bonding undergoing repulsive interaction with the neighbouring Cl. Both structures will finally yield a normal Cl⁺ beam in ESDIAD pattern.

References

[1]   D. Dijkkamp, van E. J. Loenen, A. J. Hoeven and J. Dieleman, J. Vac. Sci. Technol. A 8 (1990) 218.

[2]   R. M. Feenstra and G. S. Oehrlein, Appl. Phys. Lett. 47 (1985) 97.

[3]   R. M. Feenstra and G. S. Oehrlein, J. Vac. Sci. Technol. B 3 (1985) 1136.

[4]   V. A. Ukraintsev and J. T. Yates, Jr., Surf. Sci. 346 (1996) 31.

[5]   H. J. W. Zandvliet, H. K. Louwsma, P. E. Hegeman and B. Poelsema, Phys. Rev. Lett. 75 (1995) 3890.

[6]   K. Kato, T. Ide, S. Miura, A. Tamura and T. Ichinokawa, Surf. Sci. 194 (1988) L87.

[7]   A. E. Dolbak, B. Z. Olshanetsky, S. I. Stenin, S. A. Teys and T. A. Gavrilova, Surf. Sci. 218 (1989) 37.

[8]   H. Niehus, U. K. Kohler, M. Copel and J. E. Demuth, J. Microscopy 152 (1988) 735.

[9]   J. Wang, T. A. Arias and J. D. Joannopoulos, Phys. Rev. B 47 (1993) 10497.

[10]   J. H. G. Owen, D. R. Bowler, C. M. Goringe, K. Miki and G. A. D. Briggs, Surf. Sci. Lett. 341 (1995) 1042.

[11]   F. K. Men, A. R. Smith, K. J. Chao, Z. Zhang and C. K. Shih, Phys. Rev. B 52 (1995) 8650.

[12]   H. F. Winters and J. W. Coburn, Surf. Sci. Rep. 14 (1992) 161.

[13]   M. L. Yu and L. A. DeLouise, Surf. Sci. Rep. 19 (1994) 285.

[14]   Q. Gao, C. C. Cheng, P. J. Chen, W. J. Choyke and J. T. Yates, Jr., J. Chem. Phys. 98 (1993) 8308.

[15]   D. Sterratt, C. L. Greenwood, E. M. Williams, C. A. Muryn, P. L. Wincott, G. Thornton and E. Roman, Surf. Sci. 307-309 (1994) 269.

[16]   N. Aoto, E. Ikawa and Y. Kurogi, Surf. Sci. 199 (1988) 408.

[17] R. B. Jackman, H. Ebert and J. S. Foord, Surf. Sci. 176 (1986) 183.

[18] K. Karahashi, J. Matsuo and S. Hijiya, Appl. Surf. Sci. 60/61 (1992) 126.

[19] M. A. Mendicino and E. G. Seebauer, Appl. Surf. Sci. 68 (1993) 285.

[20] A. Szabo, P. D. Farrall and T. Engel, Surf. Sci. 312 (1994) 284.

[21] A. Szabo and T. Engel, J. Vac. Sci. Technol. A 12 (1994) 648.

[22] M. Chander, D. A. Goetsch, C. M. Aldao and J. H. Weaver, Phys. Rev. Lett. 74 (1995) 2014.

[23] S. L. Bennett, C. L. Greenwood and E. M. Williams, Surf. Sci. 290 (1993) 267.

[24] T. D. Durbin, W. C. Simpson, V. Chakarian, D. K. Shuh, P. R. Varekamp, C. W. Lo and J. A. Yarmoff, Surf. Sci. 316 (1994) 257.

[25] P. Kruger and J. Pollmann, Phys. Rev. B 47 (1993) 1898.

[26] M. W. Radny and P. V. Smith, Surf. Sci. 319 (1994) 232.

[27] Z. Dohnalek, Q. Gao, W. J. Choyke and J. T. Yates, Jr., Surf. Sci. 320 (1994) 238.

[28] F. X. Campos, G. C. Weaver, C. J. Waltman and S. R. Leone, J. Vac. Sci. Technol. B 10 (1992) 2217.

[29] C. C. Cheng, Q. Gao, W. J. Choyke and J. T. Yates, Jr., Phys. Rev. B 46 (1992) 12810.

[30] S. L. Bennett, C. L. Greenwood and E. M. Williams, DIET V (1992) .

[31] H. Nishino, W. Yang, Z. Dohnalek, V. A. Ukraintsev and J. T. Yates, Jr., submitted to J. Vac. Sci. Technol. A.

[32] M. J. Bozack, L. Muehlhoff, J. N. Russell Jr., W. J. Choyke and J. T. Yates, Jr., J. Vac. Sci. Technol. A 5 (1985) 1.

[33] A. Winkler and J. T. Yates, Jr., J. Vac. Sci. Technol. A 6 (1988) 2929.

[34] M. J. Dresser, M. D. Alvey and J. T. Yates, Jr., Surf. Sci. 169 (1986) 91.

[35] Z. Dohnalek, N. Kamoshida, H. Nishino and J. T. Yates, Jr., in preparation.

[36] W. Yang, Z. Dohnalek, W. J. Choyke and J. T. Yates, Jr., previous paper submitted to Surf. Sci.

[37] R. D. Schnell, D. Rieger, A. Bogen, F. J. Himpsel, K. Wandelt and W. Steinmann, Phys. Rev. B 32 (1994) 8057.

[38] J. S. Villarrubia and J. J. Boland, Phys. Rev. Lett. 63 (1989) 306.

[39] P. Gupta, P. A. Coon, B. G. Koehler and S. M. George, Surf. Sci. 249 (1991) 92.

[40] H. Feil, H. J. W. Zandvliet, M.-H. Tsai, J. D. Dow and I. S. T. Tsong, Phys. Rev. Lett. 69 (1992) 3076.

[41] H. J. W. Zandvliet, H. B. Elswijk, van E. J. Loehen and I. S. T. Tsong, Phys. Rev. B 46 (1992) 7581.

[42] P. Bedrosian, Surf. Sci. 301 (1994) 223.

[43] W. C. Simpson and J. A. Yarmoff, Phys. Rev. B 52 (1995) 2038.

Models of Split off Dimer Defect Structures
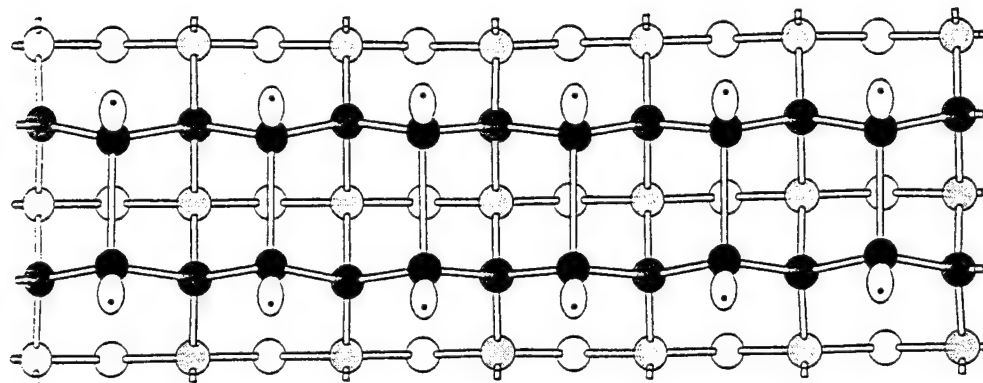
a) Part of Ideal Si(100)-(2x1) Surface

Dimer   Split off   Double Dimer
Vacancy   Dimer   Vacancy
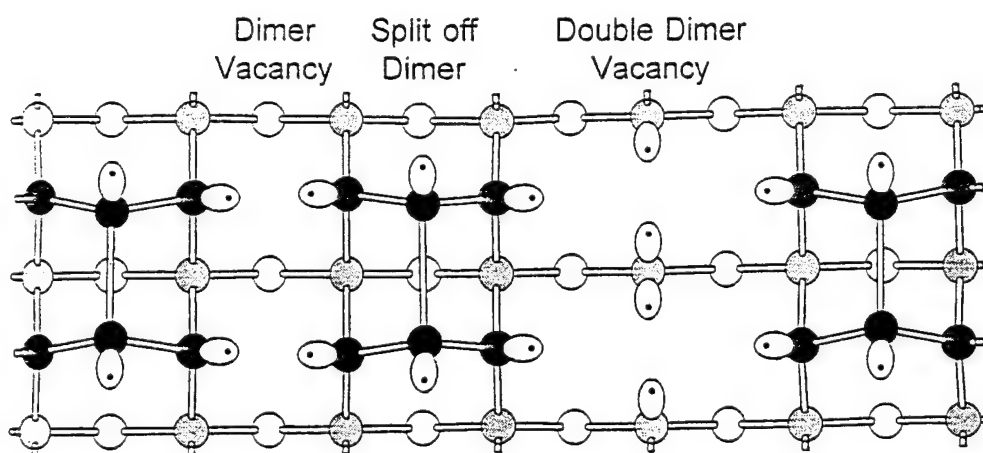
b) Split off Dimer Structure proposed by Niehus et al.
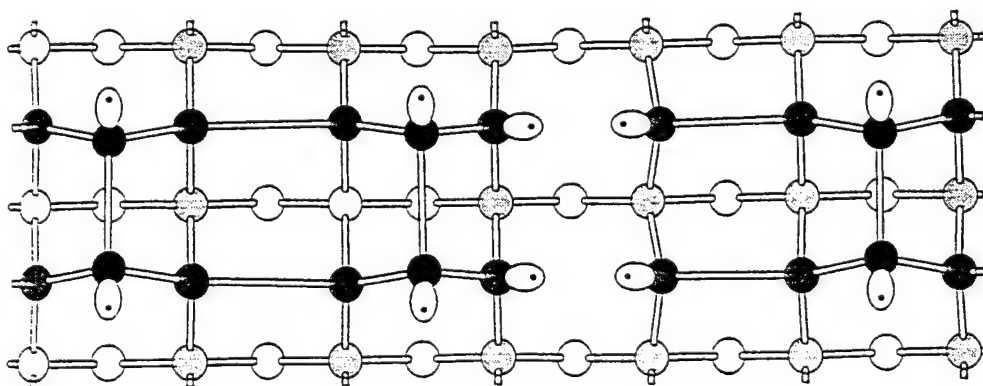
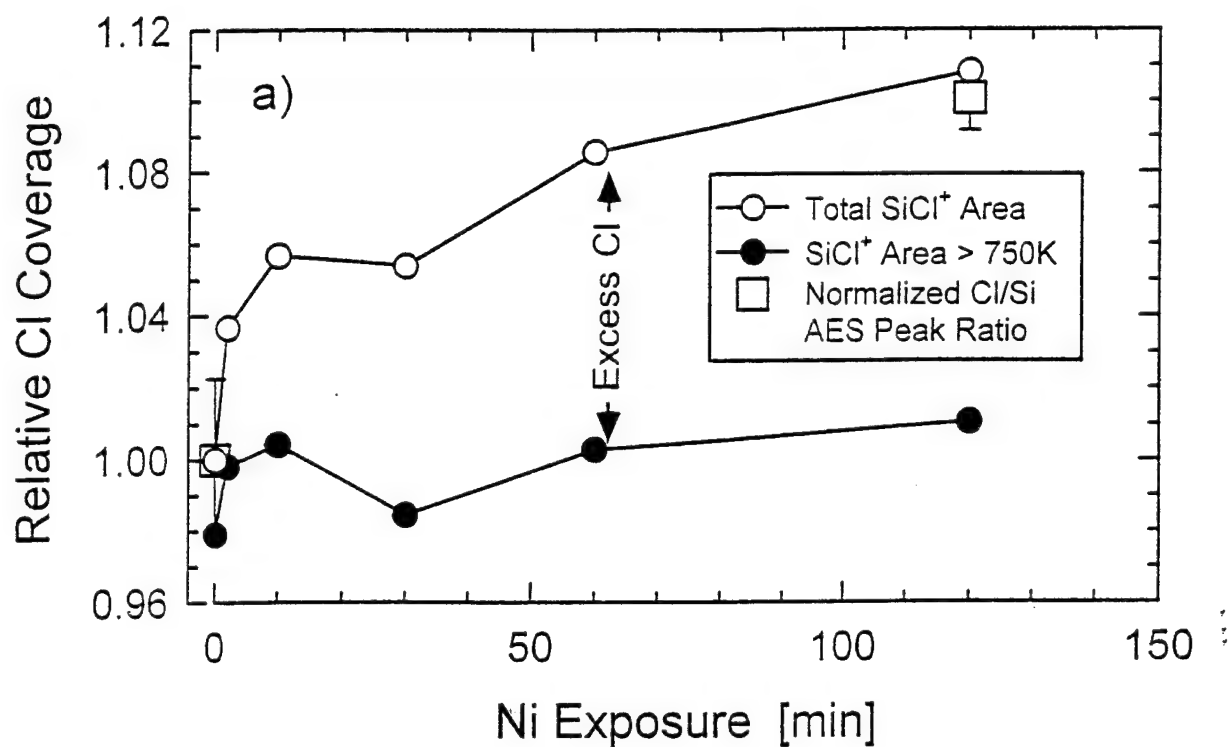c) Split off Dimer Structure proposed by Wang et al.

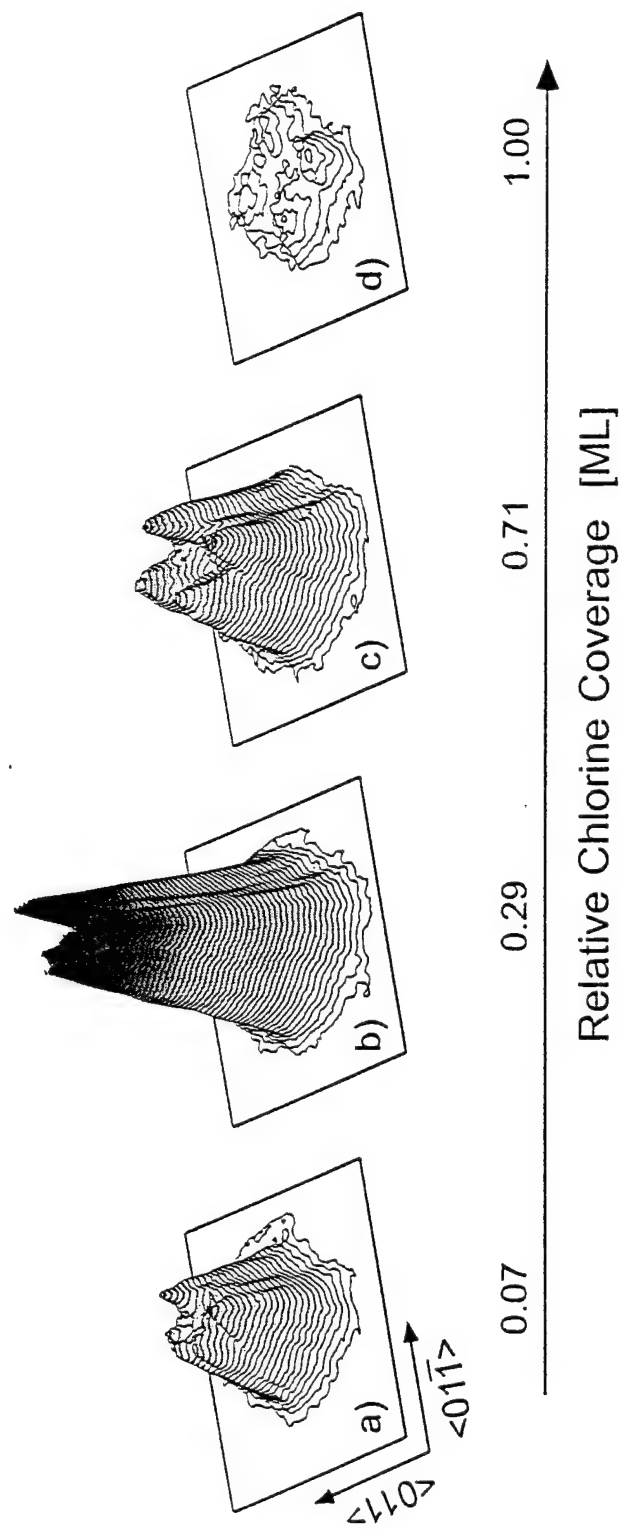SiCl₂ Desorption from Cl Saturated Si(100)-(2x1) Surface As Function of Nickel Exposure
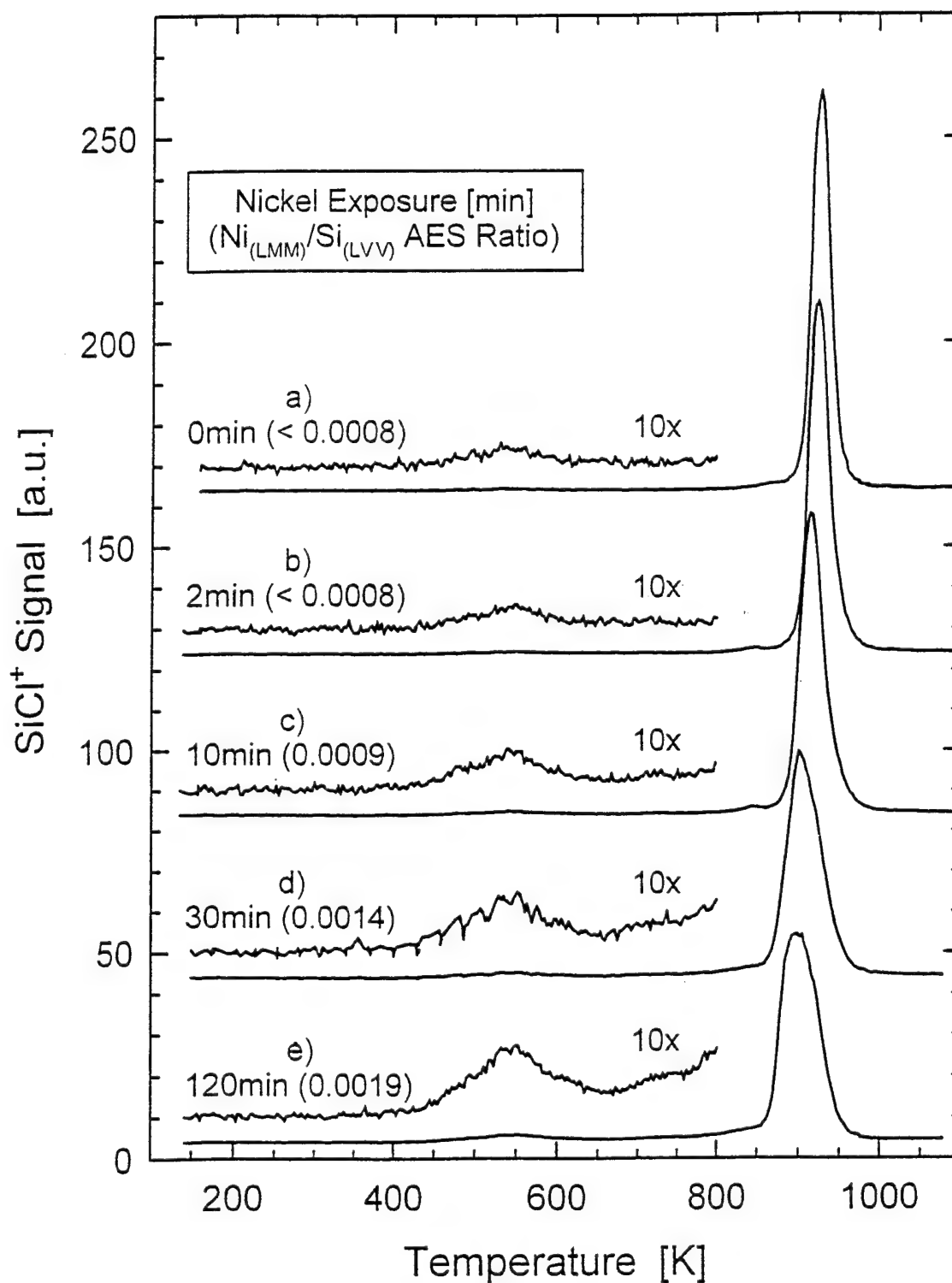
Dohnálek, et al.

Figure 2

# Relative Chlorine Coverage
as Function of Amount of Deposited Nickel
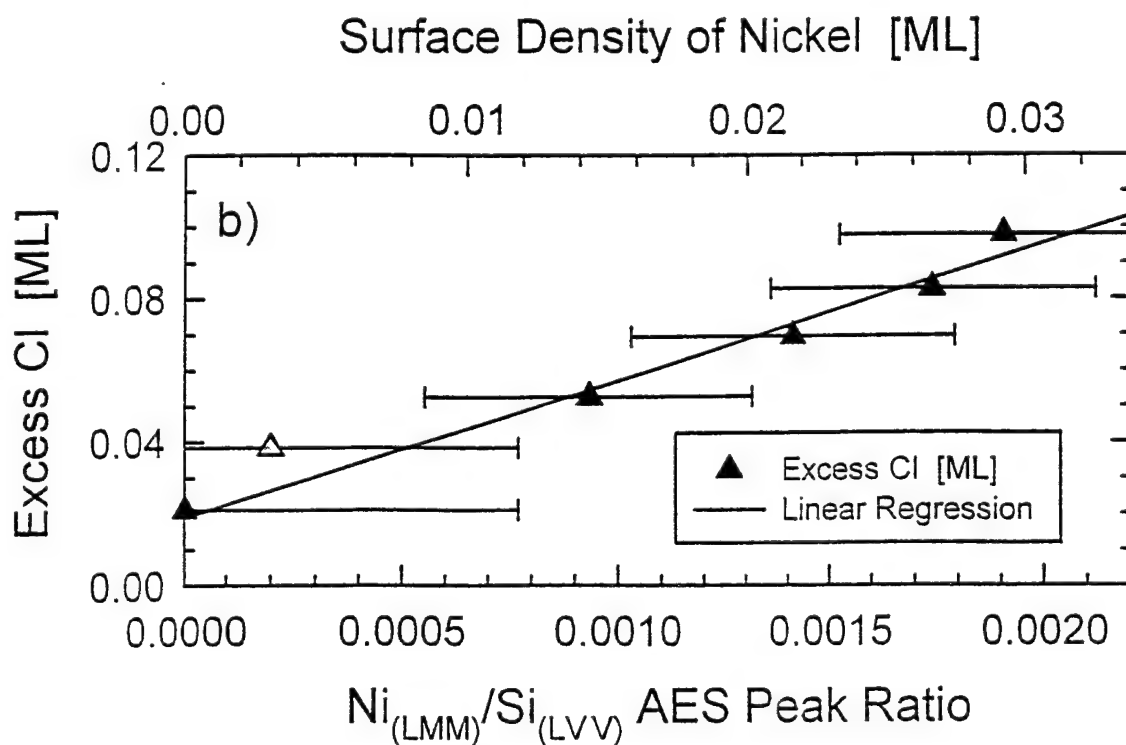
Cl+ ESDIAD Images after Chlorine Adsorption on Si(100)-(2x1) Surface at 120K


Relative Chlorine Coverage [ML]

Dohnálek,
et al.

Figure 4

Development of Cl⁺ ESDIAD Beam in Normal Direction on Chlorine Saturated Si(100) 2x1 Surface as Function of Nickel Contamination

1.00 ML of Cl/Si(100)

Cut in <011> direction

d)

Defect Density Increases
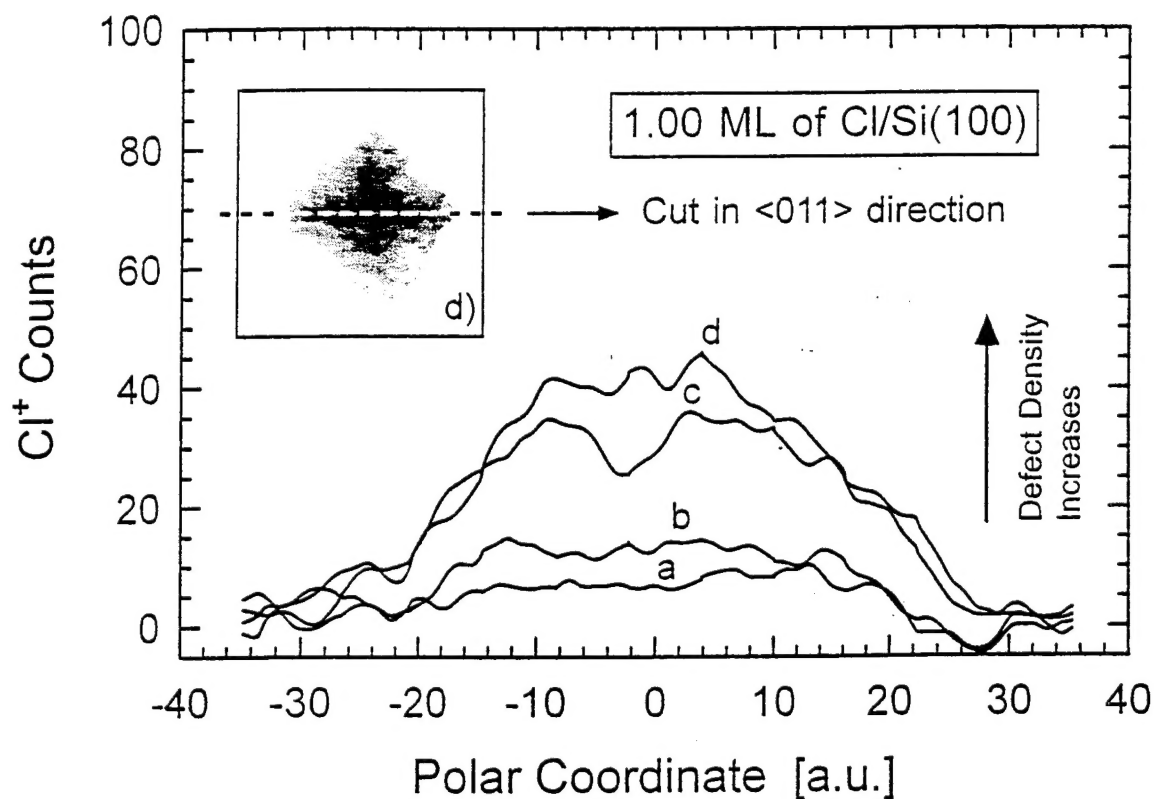
Dohnálek, et al.

Figure 5A

Development of Cl⁺ ESDIAD Beam in Normal Direction on Chlorine Covered Si(100) 2x1 Surface as Function of Nickel Contamination
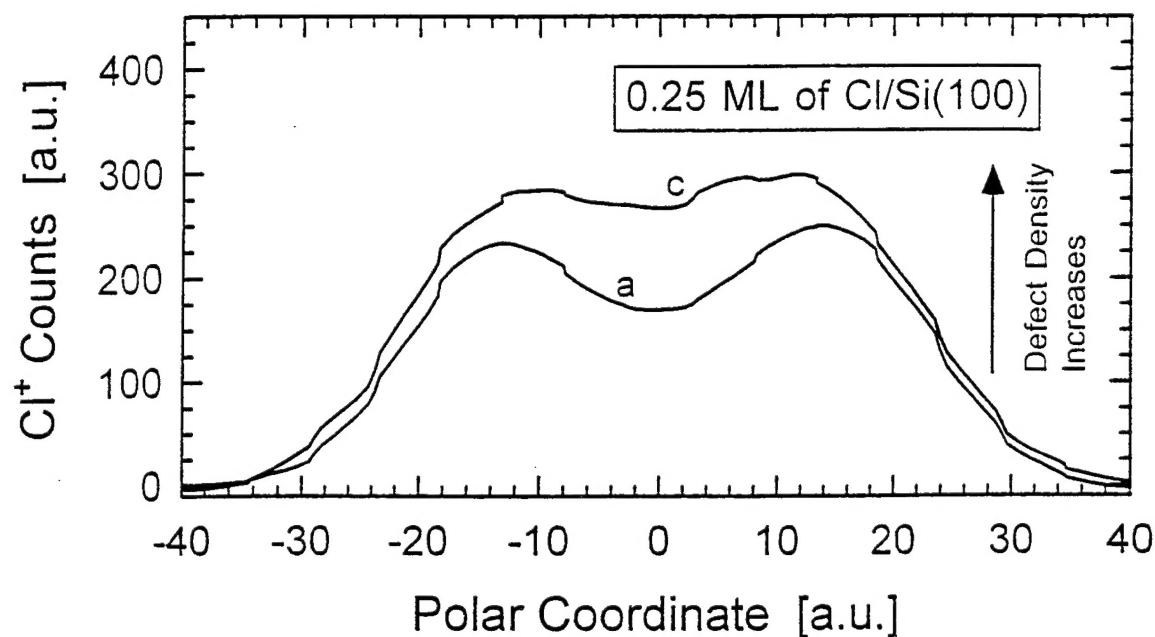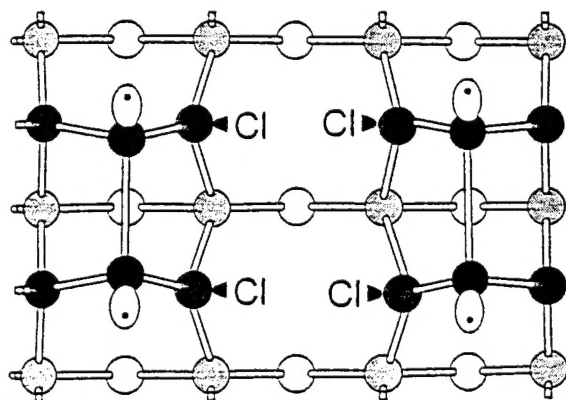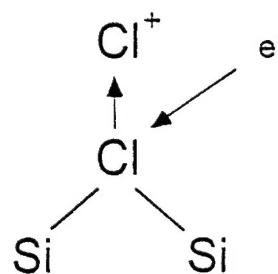
Dohnálek,
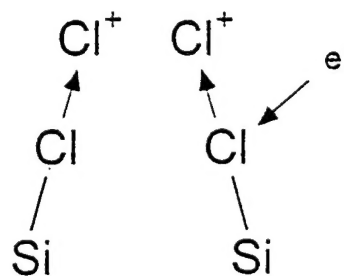et al.

Figure 5B

Models of Cl Bonding Inside of the Dimer Vacancy
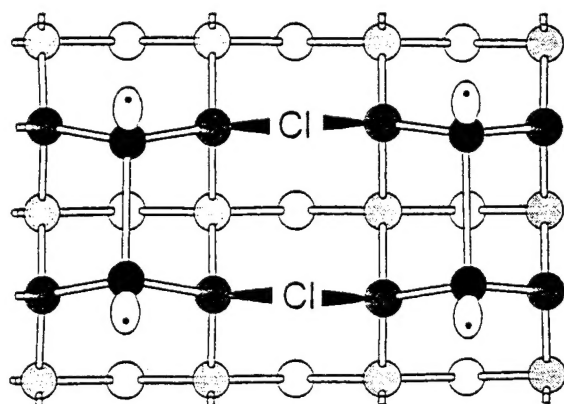
(a) Model A: Bridge-bonded Cl.

(b) Model B: Terminal Si-Cl bonds under repulsion.

Dr. John C. Pazik   (1)*
Physical S&T Division - ONR 331
Office of Naval Research
800 N. Quincy St.
Arlington, VA 22217-5660

Defense Technical Information Ctr   (2)
Building 5, Cameron Station
Alexandria, VA 22314

Dr. James S. Murday   (1)
Chemistry Division, NRL 6100
Naval Research Laboratory
Washington, DC 20375-5660

Dr. John Fischer   (1)
Chemistry Division, Code 385

NAWCWD - China Lake
China Lake, CA 93555-6001

Dr. Peter Seligman   (1)
NCCOSC - NRAD
San Diego, CA 92152-5000

Dr. Bernard E. Douda   (1)
Crane Division
NAWC
Crane, Indiana 47522-5000

* Number of copies required